01 May 2023

Dual Crosslinked Poly(acrylamide-co-N-vinylpyrrolidone) Microspheres With Re-crosslinking Ability For Fossil Energy Recovery

Jingyang Pu

Baojun Bai
Missouri University of Science and Technology, baib@mst.edu

Jiaming Geng

Na Zhang

et. al. For a complete list of authors, see https://scholarsmine.mst.edu/geosci_geo_peteng_facwork/2116

Recommended Citation

J. Pu et al., "Dual Crosslinked Poly(acrylamide-co-N-vinylpyrrolidone) Microspheres With Re-crosslinking Ability For Fossil Energy Recovery," *Geoenergy Science and Engineering*, vol. 224, article no. 211604, Elsevier, May 2023.
The definitive version is available at https://doi.org/10.1016/j.geoen.2023.211604

224 (2023) 211604

Contents lists available at ScienceDirect

Geoenergy Science and Engineering

journal homepage: www.sciencedirect.com/journal/geoenergy-science-and-engineering

Dual crosslinked poly(acrylamide-co-N-vinylpyrrolidone) microspheres with re-crosslinking ability for fossil energy recovery

Jingyang Pu [a,b,*], Baojun Bai [c], Jiaming Geng [c], Na Zhang [d], Thomas Schuman [c]

[a] College of Carbon Neutral Energy, China University of Petroleum (Beijing), Beijing, 102249, China
[b] State Key Laboratory of Petroleum Resources and Prospecting, China University of Petroleum (Beijing), Beijing, 102249, China
[c] Department of Geosciences and Geological and Petroleum Engineering, Missouri University of Science and Technology, Rolla, MO, 65409, USA
[d] Department of Energy and Mining Engineering, Shandong University of Science and Technology, Qingdao, Shandong, 266590, China

ARTICLE INFO

Keywords:
Re-crosslinkable microsphere
Dual crosslinking
Chromium acetate
Blocking agent
Network parameter

ABSTRACT

Microspheres have been proposed to be applied in controlling wastewater production for mature oilfields and migrating leakage for gas and nuclear waste storage. However, it remains challenging for stacked microspheres to maintain strong blocking ability in micron-sized small pores or fractures. In this study, a novel microsphere was developed with comprehensive properties including high deformability and long re-crosslinking time upon tunable swelling ratio for the applications. A dual covalent and physical crosslinking strategy was used to develop novel microspheres reinforced by a hydrogen bond (H-bond, between pyrrole ring and amide group) and coordination bond (between chromium acetate (CrAc) and carboxyl group via hydrolysis process). The microspheres were fabricated via radical suspension copolymerization of acrylamide (AM) and N-vinylpyrrolidone (NVP) in the presence of *N*, *N*'-methylene-diacrylamide (MBA) with subsequent introduction of CrAc. MBA induced the strong crosslinking through a chemical covalent bond and H-bond triggered the weak crosslinking which was anticipated to prohibit the hydrolysis of the amide group. The H-bond delayed the formation of CrAc coordination bond by delaying the formation of carboxyl groups, resulting in achieving the re-crosslinking of the microspheres. As a result, the microspheres exhibit the tunable initial size (8–165 μm) and swelling ratio (30–630 μm), with controllable network parameters. The microspheres showed high migration ability (can transport through pores with 1/16 size of microsphere itself), and long re-crosslinking time (up to 16.5 days). The re-crosslinked gel demonstrated dual network structure with districted mesh size ζ distribution.

1. Introduction

Polymeric microspheres are chemically or physically crosslinked polymer network microgels capable of absorbing large amounts of water (Lv et al., 2022). The polymeric microspheres have been utilized in numerous fields, such as drug delivery, food engineering, tissue engineering, and so on. The microspheres have attracted continues attention in oil recovery industry in recent years and can be utilized as blocking agents in mature unconventional reservoirs with micron-sized small pores or fractures (Bai et al., 2015; Wang et al., 2021a; Yao et al., 2015; Song et al., 2008; Wan et al., 2013; Zhao et al., 2021a) for leaking control by controlling waste water production and improving CO_2 storage efficiency (Wang et al., 2022; Xu et al., 2021). Because of their flexible size, tunable swelling and extrusion property, and good injection properties, polymeric microspheres can migrate deep into the reservoir and achieve deep profile control (Lin et al., 2015). The polymeric microspheres are usually fabricated through the approach of suspension polymerization or miniemulsion polymerization. The conventional microsphere usually exhibits poor blocking performance due to their intrinsic structural sensitivity to the reservoir and uncontrollable stacking in the target zone, which severely hinders their practical application in conformance control field such as fracture blocking (Zhu et al., 2018; Zhao and Bai, 2022a; Zhao et al., 2021b). To address this problem, tremendous efforts have been devoted to develop microspheres with multiple microstructures and low sensitivity to reservoirs, including AM/HEMA microspheres with controllable hydroxyl number (Wang et al., 2021b), hydrophobically associating polymer microspheres (named as P(AM-S)) (Wang et al., 2020a), dispersed particle gel (DPG) with improved migration ability (Varel et al., 2021),etc.

Recently, dual crosslinked hydrogels (Hu et al., 2021), which have a

* Corresponding author. College of Carbon Neutral Energy, China University of Petroleum (Beijing), Beijing, 102249, China.
E-mail address: pujyghost@163.com (J. Pu).

https://doi.org/10.1016/j.geoen.2023.211604
Received 31 May 2022; Received in revised form 9 February 2023; Accepted 20 February 2023
Available online 23 February 2023

single network with two different chemical or physical crosslinkings, have attained increasing attention because of their tunable physical/chemical properties (Wang et al., 2018a). Upon swelling, the relatively strong crosslinkings in the hydrogel is utilized to maintain the integrity, while the relatively weak crosslinkings act as sacrificial bonds or transferable bonds for energy dissipation (Li et al., 2020). Different from covalent crosslinkings, physical crosslinkings, including hydrogen-bond (H-bond), coordination bond, association bond, can recover after destruction referring to their reversible nature and is thought as ideal weak crosslinkings in the hydrogel (Rebers et al., 2021). This unstable property allows the hydrogel to self-healing upon a large deformation or disruption (Wang et al., 2018b). Thus, many non-covalent bonds such as hydrogen bonds (Gao et al., 2022), metal coordination bonds (Pu et al., 2021a), electrostatic interactions (Pu et al., 2021b) have been widely used to synthesize hydrogels with self-healing ability. We envision that, if the self-healing can be applied on microspheres which make them re-crosslink to re-form a bulky gel, it will strongly improve the blocking ability through forming a larger bulk gel in the target zones.

The coordination bonds between Cr^{3+} ions and carboxyl groups from poly(acrylamide-co-acrylic acid) chains have been widely employed to prepare in-situ gelling system in oil industry (Pu et al., 2019a). The crosslinking process can be delayed by tunable chromium crosslinkers (Zhang et al., 2020), which demonstrates potential re-crosslinking application in hydrogels. Inspired by the chromium coordination bond, in our previous reports, several metal-participated dual crosslinked hydrogels with relatively strong re-crosslinking or re-assembling properties have been synthesized (Pu et al., 2019a, 2021a; Wang et al., 2017). The coordination bond between chromium acetate or zirconium acetate with carboxyl groups served as sacrificial bonds to release re-crosslinking. However, the re-crosslinking properties cannot be efficiently transferred to polymeric microspheres to obtain delayed in-situ re-crosslinking of the microspheres. In processes of emulsion polymerization or suspension polymerization, it was found that the metal crosslinking agent completely reacted with carboxyl group during the long synthesis process. Delaying the coordination reaction between Cr^{3+} ions and carboxyl groups remains a challenge.

Poly(N-vinylpyrrolidone) have become a polymeric material in tertiary oil recovery which are mainly applied for high temperature reservoirs (Wang et al., 2018a). pyrrole ring of Poly(N-vinylpyrrolidone) have been reported which can form strong cooperative H-bonds with amide groups of polyacrylamide or poly(acrylamide-co-acrylic acid) to improve the temperature tolerance (Lin et al., 2015; Guo et al., 2020; Wang et al., 2020b). It is believed that the temperature tolerance of the microspheres resulted from the inhibition ability of H-bond to the hydrolysis of amide group. Very little work has been done on using H-bond between pyrrole ring and amide group to delay the formation of carboxyl group and promote the delay re-crosslinking of the microsphere.

Inspired by above-mentioned studies, we intended to fabricate novel re-crosslinkable microspheres (MRPG) that are covalent crosslinked by *N*, *N*'-methylene-diacrylamide (MBA) maintain the integrity and coordination bonds between CrAc and carboxyl group from hydrolyzed poly (acrylamide-co-N-vinylpyrrolidone) to obtain microspheres exhibit both high deformability (can transport 1/16 size of microsphere itself) and delayed re-crosslinking time. To this end, radical suspension copolymerization of acrylamide (AM) and N-vinylpyrrolidone (NVP) and subsequent introduction of CrAc were carried out, with MBA and H-bond (formed by pyrrole ring and amide group) triggering the dual crosslinking of polymer networks. The microspheres with size ranged from 8 to 165 μm were fabricated from W/O suspension copolymerization whose droplet was larger than miniemulsion and microemulsion. The H-bond were anticipated to serve as an inhibition to the polymer hydrolysis and the formation of carboxyl group. The delayed formation of intra-coordination bonds was expected to endow the microspheres with re-crosslinking ability, upon swelling and deformability. The structure and morphology of the microspheres were characterized, combined with the network parameter study. Their integrity, temperature resistance, migration and deformability behaviors, and re-crosslinking behaviors were evaluated and discussed.

2. Materials and methods

2.1. Materials

AM, NVP, chromium acetate ($[CH_3COO]_7[OH]_2Cr_3$, Cr^{3+} 24%), and n-Decane(ACS-grade) were provided by Alfa Aesar. MBA and sorbitane mono-oleate (Span80) were obtained from Sigma Aldrich. Ammonium persulfate (APS), potassium persulfate (KPS), and ACS-grade acetone were purchased from Fisher Scientific. All reagents were used as received unless specified.

2.2. Preparation of MRPG microspheres

A typical MRPG microsphere preparation procedure followed our earlier report (Pu et al., 2019b): An aqueous phase solution was first prepared by dissolving the monomer AM (4.22 mol/L), NVP (0.337 mol/L), MBA (0.485 mmol/L), and chromium acetate ([Cr(III)] = 0.2 mol/L) in 8 ml of deionized water. The 50% APS solution and 50% KPS solution were prepared separately. The aqueous solution was poured into a 100 ml three-necked round-bottomed flask with the organic continuous phase comprising 50 ml of *n*-decane and 2 g of Span80 to prepare a W/O mixture. The mixture was emulsified for 120 s by using an Ultra-Turax (9000 rpm) homogenizer before the addition of 0.35 ml of APS solution and KPS solution separately. Then, the flask was equipped with a mechanical stirrer, a reflux condenser, a thermometer, and a nitrogen inlet and subsequently placed carefully in a constant-temperature water bath (50 °C) for 12 h with 600 rpm stirring for complete polymerization. The volume of the final solid product was controlled between 5 and 10 g. The product was washed twice with acetone.

All of the washed microspheres were dried at 50 °C for another 12 h. The microspheres were weighed to a constant mass (W_i) before being dispersed in water. The dispersion was kept for 5 days with occasional shaking to remove water-soluble components from the microspheres. The insoluble component was further dried in a vacuum oven to a final constant weight (W_d). Yield ratio (Yield%) was obtained as

$$\text{Yield}\% = \frac{W_d}{W_i} \times 100 \quad (1)$$

Gel ratio (Gel%) was obtained as

$$\text{Gel}\% = \frac{W_d}{W_a} \times 100 \quad (2)$$

where W_a is the total weight of the monomers and crosslinkers (AM, NVP, chromium acetate, and MBA) taken for the synthesis of the microspheres.

2.3. Characterization of the microspheres

2.3.1. Structure and morphology of the microspheres

The morphology of the MRPG microspheres was observed with a Hitachi S4700 scanning electron microscope (SEM). The fully swollen microspheres were lyophilized and sprayed with Au–Pd before the observation. In detail, the microspheres swelled after equilibrium to reveal their final crosslinked network structure in DIW or other solvent. The microsphere solutions were measured using SEM again and then lyophilized in a Christ Alpha 2–4LD device (SciQuip, Newtown, UK) for 24 h for SEM measurement. The size (diameter) distribution of the dry microspheres was obtained from SEM results by using image capture software. The size distributions of the swelling microspheres at

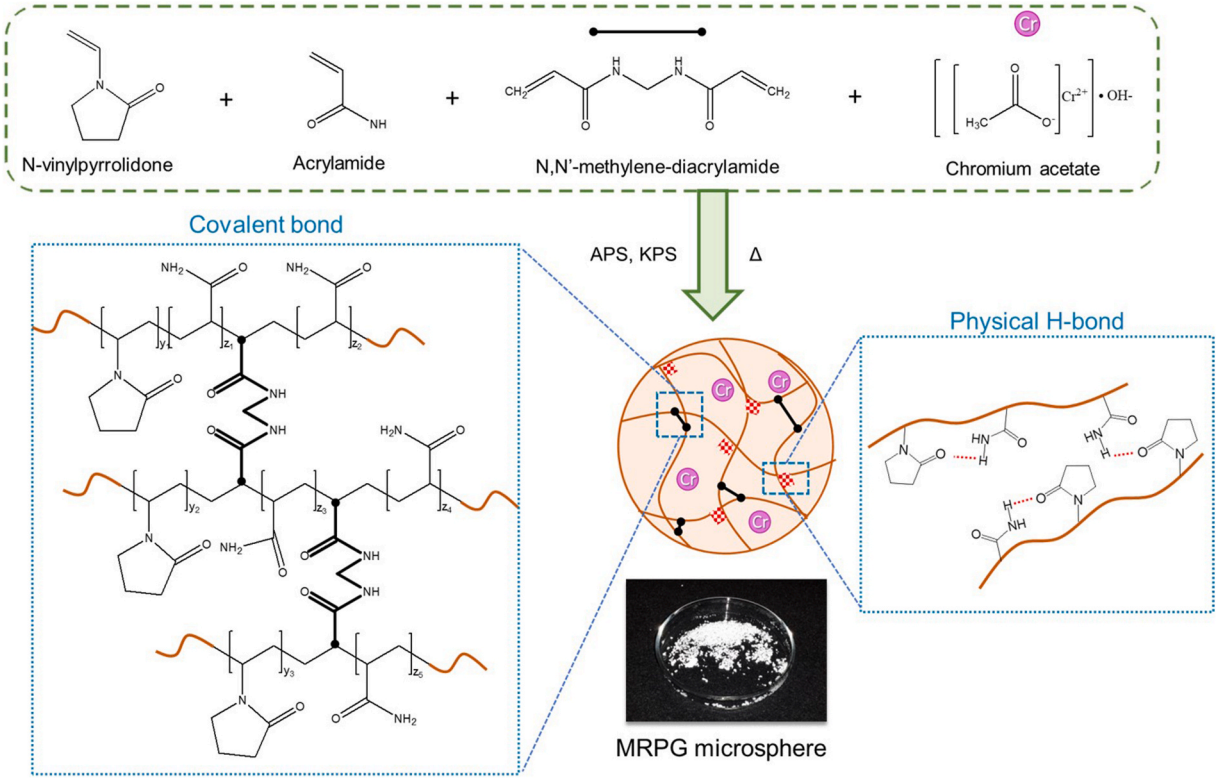

Fig. 1. Schematic of synthesis and structural formula of MRPG microspheres.

equilibrium were measured in simulated 2% NaCl brine by using a Microtrac 3000 Laser-light Scattering (LLS) apparatus.

2.3.2. Polymeric structure study with FT–IR analysis

The microsphere samples for FT–IR detection were prepared via the potassium bromide (KBr) pellet method and subsequently heated at 120 °C for 48 h to remove most of their water content. FT–IR spectra were recorded by using a Thermo Nicolet Nexus 470 spectrometer (Thermo Scientific Inc.) and processed with Omnic software.

2.4. Network parameters of the microspheres

The average molecular weights ($\overline{M}$) between crosslinks of the microsphere was obtained from swelling data by using the Flory–Rehner equation (Samanta and Ray, 2014; Flory and Rehner, 1943):

$$\overline{M} = -\frac{\nu_s \rho_p \left(\phi_{p,m}^{\frac{1}{3}} - \frac{\phi_{p,m}}{2}\right)}{\ln(1-\phi_{p,m}) + \phi_{p,m} + \chi\phi_{p,m}^2} \tag{3}$$

where ν_s is the molar volume of a solvent molecule (2% NaCl brine in this study), which was calculated as 18.2 cm^3/mol on the basis of the density (~1 g/cm^3) and molecular weight (18 g/mol) of the solvent (Mandal et al., 2012). In addition, for the equilibrium swelling of m_w, the polymer volume fraction of a fully swelling gel (at equilibrium) $\phi_{p,m}$ is

$$\phi_{p,m} = \left(1 + \frac{\rho_p}{\rho_i} m_w\right)^{-1} \tag{4}$$

where ρ_p and ρ_i are density of the polymer and brine, respectively. The swelling ratio was calculated with Equation (5) as follows:

$$SR = \frac{1}{\phi_{p,m}} \tag{5}$$

The Flory–Huggins interaction parameter χ (or the solubility parameters of the solvent and polymer) can be estimated with

$$\chi = \frac{1}{2} + \frac{\phi_{p,m}}{3} \tag{6}$$

The crosslinking density (ρ_c) of a polymeric microsphere is obtained as

$$\rho_C = \frac{\rho_p N_A}{\overline{M}} \tag{7}$$

where N_A is Avagadro's number (6.02×10^{23}/mol). The mesh size ζ in nm of the swollen polymeric network is calculated by using Equation (8).

$$\zeta = \left[C_n \left(\frac{2\overline{M}}{M_r}\right)\right]^{1/2} l\phi_p^{-1/3} \tag{8}$$

where Flory's characteristic ratio C_n is taken from the literature as 2[34]. The carbon–carbon bond length l was assumed to be 0.154 nm (1.54 Å) (Mandal et al., 2012). M_r, the molecular weight of the repeating unit, was calculated as the weight average of the repeating unit of AM (M_r = 71.08) and NVP (M_r = 111.14), which was 76.17. The values of all of these microsphere network parameters before and after re-crosslinking were calculated by using Equations (3)–(8).

2.5. Cr^{3+} diffusion study through membrane dialysis experiments

A membrane dialysis system that contained RC tubing and 200 ml of buffer was applied to measure the degree of Cr^{3+} loss from the microspheres (Pu et al., 2018). In detail, 0.1 g of dry MRPG microspheres with an initial Cr^{3+} content of approximately 10 mg was placed in a 40 ml membrane bag (Spectra/Por Standard RC Tubing) and immersed in 2% NaCl brine (Gales et al., 1994). The Cr^{3+} concentration of the dialysate was measured by using a Perkin–Elmer model 3110 atomic absorption spectrophotometer with a 359 nm laser light source at 23 °C. The cumulative amount of released Cr^{3+} was recorded and calculated by

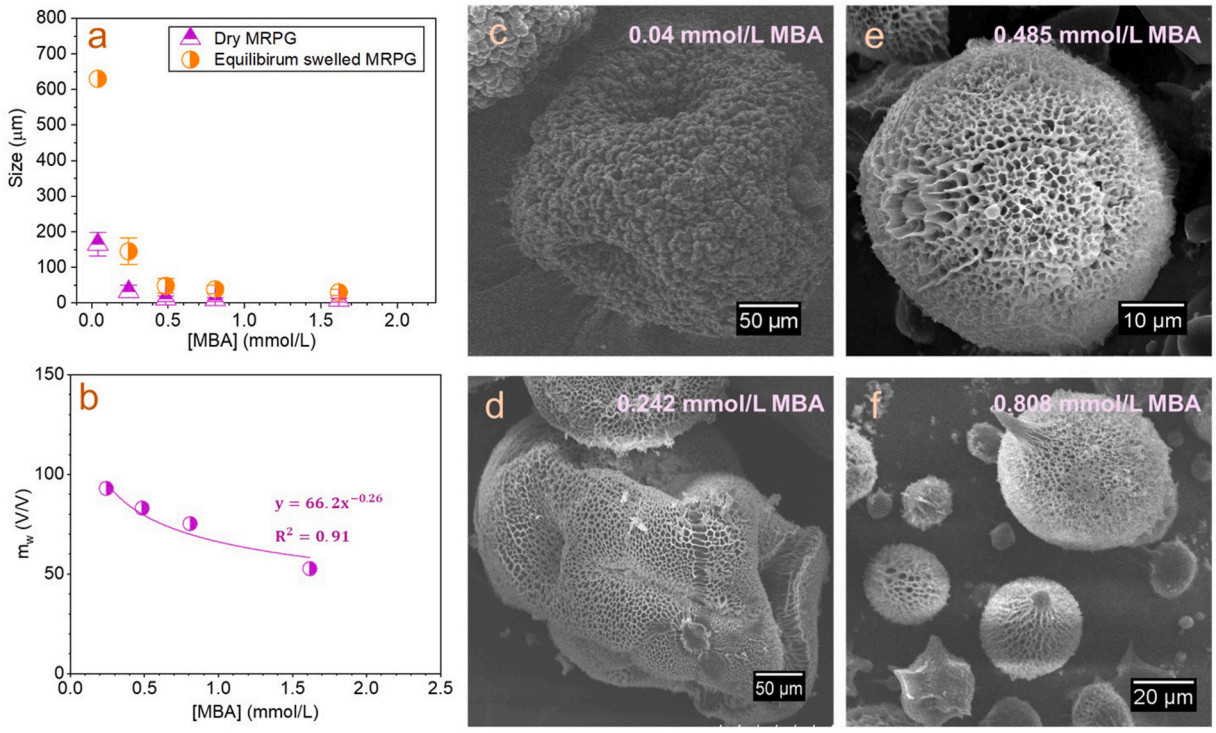

Fig. 2. Equilibrium swelling and SEM observation images of MRPG microspheres: (a) Particle size; (b) equilibrium swelling ratio m_w of the MRPG microspheres; equilibrium swelling morphologies of the microspheres (lyophilized) with the MBA concentrations of (c) 0.04 mmol/L, (d) 0.242 mmol/L, (e) 0.485 mmol/L, and (f) 0.808 mmol/L.

integrating the Cr^{3+} concentrations of the dialysate.

2.6. Temperature resistance study with thermogravimetric analysis

Thermogravimetric analysis (TGA, TA Q2000) was employed to obtain the decomposition behavior of the MRPG microspheres when heated in oxygen at the heating rate of 10 °C/min.

2.7. Migration performance and deformability with membrane filtration experiment

Nuclear-pore membranes (Isopore™ Membrane Filters, Merk Millipore Ltd.) were applied in the filtration experiment to investigate the migration of the MRPG microspheres through pores (Zhao and Bai, 2022b). A dispersion of the microspheres was prepared by dispersing dry microspheres into 2% NaCl brine. The dispersion was stirred for 2 h at room temperature and was subsequently transferred at a certain rate into a beaker through a nuclear-pore membrane system with a variety of pore sizes (1.2, 3, 5, and 10 μm) under a differential pressure of 15 psi. The migration ability of the MRPG was studied by investigating the cumulative volume of the produced solution as a function of time.

2.8. Determination of re-crosslinking time

The effect MBA concentrations, NVP concentrations, and temperature on the re-crosslinking properties of the microspheres were investigated. The dry sample was directly observed through SEM and was suspended in acetone for CLSM (Nikon Tie motorized microscope equipped with a Yokagowa X1 confocal scan head and four lasers with AOTF control. For CLSM observation, one drop of the sample was placed on the clean surface of a glass slide. For example, Microsphere dispersions with the concentration of 5000 mg/l were prepared under sonication to obtain the equilibrium swollen microsphere solution. The dispersions were sealed in bottles and placed in a water bath at different

Table 1
Size and swelled network mesh size distribution of the MRPG microspheres.

Type	[MBA] (mmol/L)	[NVP] (mol/L)	Stirring rate (rpm)	Dry size, exp. (μm)	Swelled size, exp. (μm)	m_w (V/V)	ζ_{exp} (nm)	ζ_{cal} (nm)	Pore threshold (μm)	Pore cannot be transported
MBA conc.	0.040[a]	0.337	600	165	630	55.7	–	1614.4	39.4	15.8
	0.242	0.337	600	32	145	93.0	4210.5	4873.8	9.1	3.6
	0.485	0.337	600	11	48	83.1	1443.5	3820.0	3.0	1.2
	0.808	0.337	600	9	38	75.3	1328.5	3087.9	2.4	1.0
	1.617	0.337	600	8	30	52.7	1003.9	1437.7	1.9	0.8
NVP conc.	0.485	0.171	600	10	46	132.7	2750.2	5372.3	2.9	1.2
	0.485	0.337	600	11	48	83.1	1443.5	3820.0	3.0	1.2
	0.485[a]	0.450	600	25	33	2.3	–	2.7	2.1	0.8
Stir rate	0.485	0.337	500	13	44	38.8	1022.1	744.5	2.8	1.1
	0.485	0.337	600	11	48	83.1	1443.5	3820.0	3.0	1.2
	0.485	0.337	700	10.6	46	81.7	1568.4	3686.2	2.9	1.2
	0.485	0.337	850	10.5	47	89.7	2259.4	4503.4	2.9	1.2

[a] ζ_{exp} of the samples are unavailable due to excessive deformability.

Table 2
Network parameters, Yield%, and Gel% of the MRPG microspheres.

Type	[MBA] (mmol/L)	[NVP] (mol/L)	$\phi_{p,m}$ ($\times 10^{-2}$)	SR	$\overline{M}$ ($\times 10^{7}$)	χ	ρ_C ($\times 10^{15}$)	Yield%	Gel%
MBA conc.	0.040	0.337	1.9	53.9	14.7	0.5062	3.90	75	55
	0.242	0.337	1.1	89.4	95.4	0.5037	0.60	87	70
	0.485	0.337	1.3	79.9	63.1	0.5042	0.91	89	75
	0.808	0.337	1.4	72.5	44.0	0.5046	1.30	93	87
	1.617	0.337	2.0	51.1	12.1	0.5065	4.75	90	81
NVP conc.	0.485	0.171	1.1	93.5	112.5	0.5036	0.51	91	82
	0.485	0.337	1.3	79.9	63.1	0.5042	0.91	89	75
	0.485[a]	0.450	31.4	3.2	0.0	0.6047	206226.3	45	61
Stir rate	0.485	0.337	2.6	37.8	3.9	0.5088	14.48	87	76
	0.485	0.337	1.3	79.9	63.1	0.5042	0.91	89	75
	0.485	0.337	1.3	78.6	59.4	0.5042	0.96	87	74
	0.485	0.337	1.2	86.2	83.4	0.5039	0.69	88	70

[a] $\phi_{p,m}$, SR, $\overline{M}$, χ, and ρ_C of the sample is abnormal due to the sample's excessive deformability.

temperature (50 °C, 65 °C, 80 °C, and 100 °C). The sizes of the dispersed and swollen microspheres were observed through SEM (in the lyophilized state) and CLSM (in the equilibrium water absorption state) and the re-crosslinking time of the microsphere was defined as when the measured size increased for the first time.

3. Results and discussion

3.1. Analysis of lateral chain structures

The schematic illustration of the fabrication of covalent crosslinked P(AM-c-NVP) microsphere hydrogels is shown in Fig. 1. Radical suspension copolymerization of acrylamide (AM) and N-vinylpyrrolidone

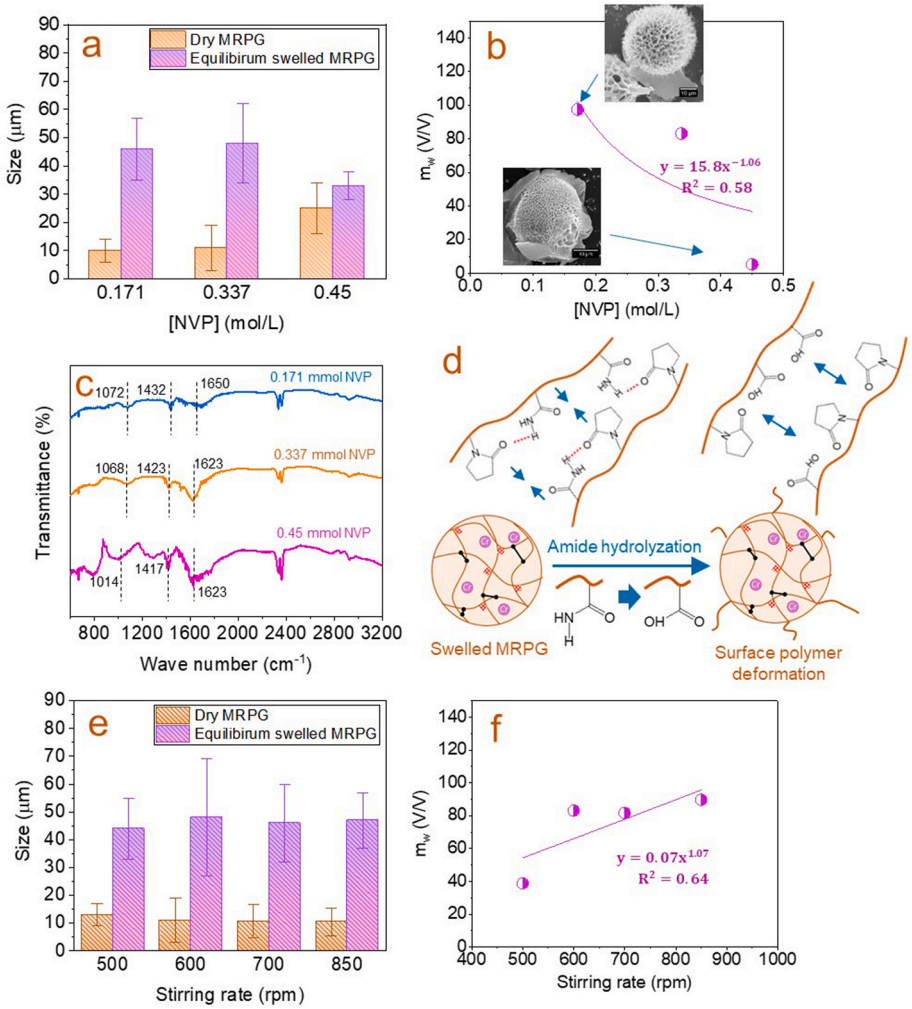

Fig. 3. Swelling and FT-IR measurement of MRPG microspheres: Particle size (a) and equilibrium swelling ratio m_w (b) of the microspheres with different MBA concentration; FT-IR spectra of the microspheres (c) and the relationship of H-bond and coordination bond (d); Particle size (a) and equilibrium swelling ratio m_w (b) of the microspheres with different NVP concentration.

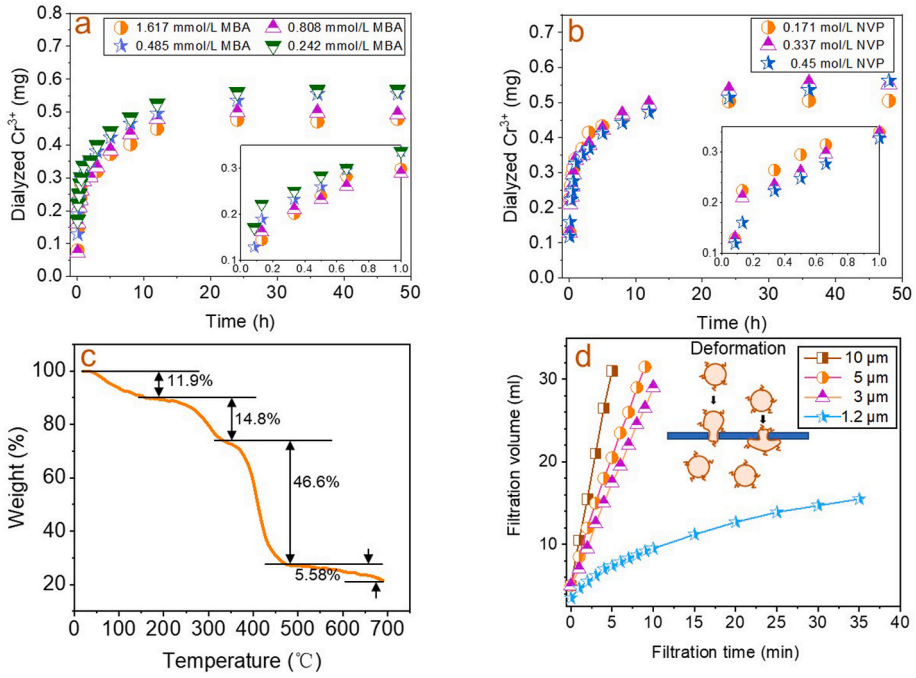

Fig. 4. Characterization of the microspheres: Dialysis analysis with different MBA concentration (a) and NVP concentration (b); TGA analysis result (c); Cumulative volume filtered through membranes with different pore sizes (d).

(NVP) were carried out with the MBA covalent crosslinkings to obtain the dual crosslinking of polymer networks with physical H-bond formed by pyrrole ring and amide group. The introduced CrAc was sealed in the polymeric network without any reactions since no carboxyl group was created from the hydrolysis process of the amide groups at early period.

3.2. Swelling behavior and network parameters of MRPGs

Crosslinker concentration controlled the overall crosslinking density in the final network structure of the microspheres. In our previous research, the microspheres exhibited micron-sized particles and good deformability after fully swollen (Pu et al., 2019c). Given that the microspheres were synthesized via the polymerization of monomer units and the covalent crosslinker MBA, the crosslinker concentration strongly affected the microsphere sizes. Fig. 2a shows the sizes of the microspheres crosslinked by using various concentrations of MBA. The dry sizes considerably reduced from 165 μm to 8 μm as the concentration of MBA was increased from 0.04 mmol/L to 1.617 mmol/L mg. Subsequently, the sizes of the equilibrium swollen microspheres decreased from 630 μm to 30 μm. The theoretical mesh sizes (ζ_{cal}) of the microspheres were calculated by using Equation (8), and the results are listed in Table 1. The average mesh sizes, named as experimental mesh size (ζ_{exp}), measured from SEM images by utilizing IMAGEJ software are also listed in Table 1 for comparison. The results showed that all of the ζ_{exp} values were less than ζ_{cal} values likely because ζ_{exp} were measured from lyophilized samples whose networks, to some extent, shrunk after lyophilization. The change trend of m_w is illustrated in Fig. 2b, and the fitted curve followed the equation of

$$m_w = kC_{MBA}^{-n} \tag{9}$$

where k = 69.97 and n = 0.263. Such behavior has been reported by pioneering work (Çaykara and Turan, 2006).

The morphologies of the samples with different concentration of MBA were demonstrated as Fig. 2c–f. The ζ_{exp} value of 0.04 mmol/L MBA microsphere were not included which had an abnormal swelling morphology as depicted in Fig. 2c. The swollen microspheres exhibited an intestine-like structure instead of a normal three-dimensional network structure. Except for this one, all of the other samples presented highly ordered structures with clear boundaries, good dispersibility, and no obvious adhesion between each other. The lyophilized microspheres also had perfect regular network structures as shown in Fig. 2d–f. The microspheres with 0.485 mmol/L of MBA showed the best sphericity among all of the microspheres.

The network parameters of the microspheres with different MBA crosslinker concentrations were provided in Table 2. The samples, except for the sample with 0.04 mmol/L of MBA as mentioned previously, showed increased $\overline{M}$ as $\phi_{p,m}$ decreased. ρ_C had a reciprocal relationship with $\overline{M}$. No effective network structure formed in the 0.04 mmol/L samples. This phenomenon resulted in the inhibition of the swelling and formation of the normal networks of the samples. The Flory–Huggins interaction parameter χ for all the samples remained constant between 0.50 and 0.51. In addition, Yield% and Gel% obviously increased as the MBA concentration in the microspheres was increased from 0.04 mmol/L to 0.808 mmol/L. However, when 1.617 mmol/L of MBA was used, Yield% and Gel% decreased because a tight network structure, which inhibited the formation of regular whole structures, formed at an early stage of polymerization (Mandal and Ray, 2013).

Besides MBA concentration, the effect of NVP concentration and stirring rate on size and m_w of the microspheres was investigated separately to study the swelling performance with various polymerization conditions. First, the effect of NVP concentration on the sizes was obtained and the result was shown in Fig. 3a. The dry size increased from 10 μm to 25 μm as the increase of NVP concentration from 0.171 mol/L to 0.45 mol/L, while the equilibrium swelled size decreased from 46 μm to 33 μm. The change trend of m_w is illustrated in Fig. 3b, which didn't fit well by Equation (9) since the m_w of the microsphere with 0.45 mol/L NVP showed abnormal low m_w when comparing with others. Other network parameters of the microsphere as shown in Table 2 reflected that when the concentration of NVP reached 0.45 mol/L, the microsphere became too soft to uptake water and the network can not completely unfold.

The presence of various chemical functional groups in MRPG microsphere was detected via FT–IR spectroscopy, and the results were

shown in Fig. 3c. Three samples with different NVP concentration were characterized since the peaks of functional groups were affected by both physical H-bond (large lateral pyrrole ring with amide group) and inter-coordination reactions (chromium acetate with carboxyl group formed via hydrolysis of amide group). It was noted that the three functional peaks (1072 cm^{-1}, 1432 cm^{-1}, and 1650 cm^{-1}) were red-shifted as the increase NVP concentration proving the existence of H-bond in the microsphere (Fig. 3d). The peaks between 1600 cm^{-1} and 1700 cm^{-1} were assigned to the stretching vibration of the C═O bonds. The lateral chains of AM and NVP had different C═O bonds. In a previous study, the peak observed in pure NVP at 1645 cm^{-1} that was due to C═O bonds red-shifted to 1560 cm^{-1} as a result of the H-bond with amide group (Sudha and Rajarajan, 2013). In the 1200 cm^{-1} to 1500 cm^{-1} region, the absorption bands of lateral chains on poly(AM-c-NVP) overlapped with the bands of chromium acetate, and inter-coordination occurred between these molecules. As the hydrolysis of amide group, more carboxyl group were formed which can coordinate with CrAc to form a physical complex structure. As the decrease of H-bond, the microsphere became softer than before. This physical coordination phenomenon helped prevent chromium acetate molecules from breaking away from the microspheres. Therefore, a wide band with its minimum at 1417 cm^{-1} and its maximum at 1432 cm^{-1} was observed for the samples with different NVP concentration. Other important doublet peaks between 1014 cm^{-1} and 1072 cm^{-1} were contributed by the amide group.

Second, the effect of stirring rate on size and m_w were investigated by preparing the microspheres with stirring rate ranging from 500 to 800 rpm. The result was shown in Fig. 3e and f, respectively. It was found that the stirring rate didn't affect the size and m_w when it was higher than 500 rpm. Other network parameters of the microsphere were listed in Table 2. At 500 rpm, it was noted that the initial size of the microsphere was larger than others while the equilibrium swollen size was smaller than others. Therefore, m_w of 500 rpm sample was only 38.8, less than half of other microspheres prepared with higher stirring rate.

3.3. Analysis of Cr^{3+} diffusion from the microspheres

The Cr^{3+} diffusion of the microspheres with different concentration of MBA were conducted to study the loss of the CrAc. CrAc exchange is an inverse process of chromium acetate coordinated with the carboxyl group on the lateral chain of poly(AM-c-NVP). As shown in Fig. 4a, the dialyzed mass of Cr^{3+} increased fast in first 5 h and became equilibrium after 30 h. The final dialyzed mass of Cr^{3+} decreased (0.58–0.47 mg) as the MBA concentration increase from 0.242 mmol/L to 1.617 mmol/L. It was noted from Table 1 that the Cr^{3+} loss amount increased as the decrease of ζ value. The NVP concentration showed a more complex effect on Cr^{3+} diffusions as shown in Fig. 4b. The final dialyzed mass of Cr^{3+} decreased (0.58–0.5 mg) as the decrease of the NVP concentration (0.45–0.171 mol/L) referring to the ζ reduction. However, the sample with smallest concentration of NVP (0.171 mol/L) dialyzed Cr^{3+} fastest in first 10 h. This phenomenon can be explained by the H-bond of pyrrole ring with amide group as mentioned in Fig. 3d. The H-bond prohibit the hydrolysis of the amide group and reduce the initial number of carboxyl groups, leaving a large number of CrAc unbound. The unbound CrAc diffused much faster from the microsphere. For all the samples, the total amount of dialyzed Cr^{3+} was less than 0.58 mg, which was a small amount, compared with the initial total amount of Cr^{3+} (10 mg). Therefore, the Cr^{3+} loss through diffusion would not affect the re-crosslinking properties of the microspheres.

As shown in Table 1, the swollen microsphere can transport through 1/16 size of microsphere itself, which means they can enter pores ranged from 1.9 to 39.4 μm pores referring to swollen size in Table 1. However, it was found from Fig. 4d that the microspheres cannot freely transport through 1/40 size (3 μm pore) of microsphere itself. The cutoff size were applied to all the prepared samples as demonstrated in Table 1, of which "pore threshold" size means the minimum size of pores allow the pass of the microspheres and "pore cannot be transported" size means the minimum size of pores don't allow the pass of the microspheres.

3.4. Temperature resistance of the microspheres

The microsphere with the 0.485 mmol/L MBA and 0.337 mol/L NVP was chosen for temperature resistance characterization and other further characterization to its good swelling behavior and network parameters. As displayed in Fig. 4c, the weight loss of the microspheres can

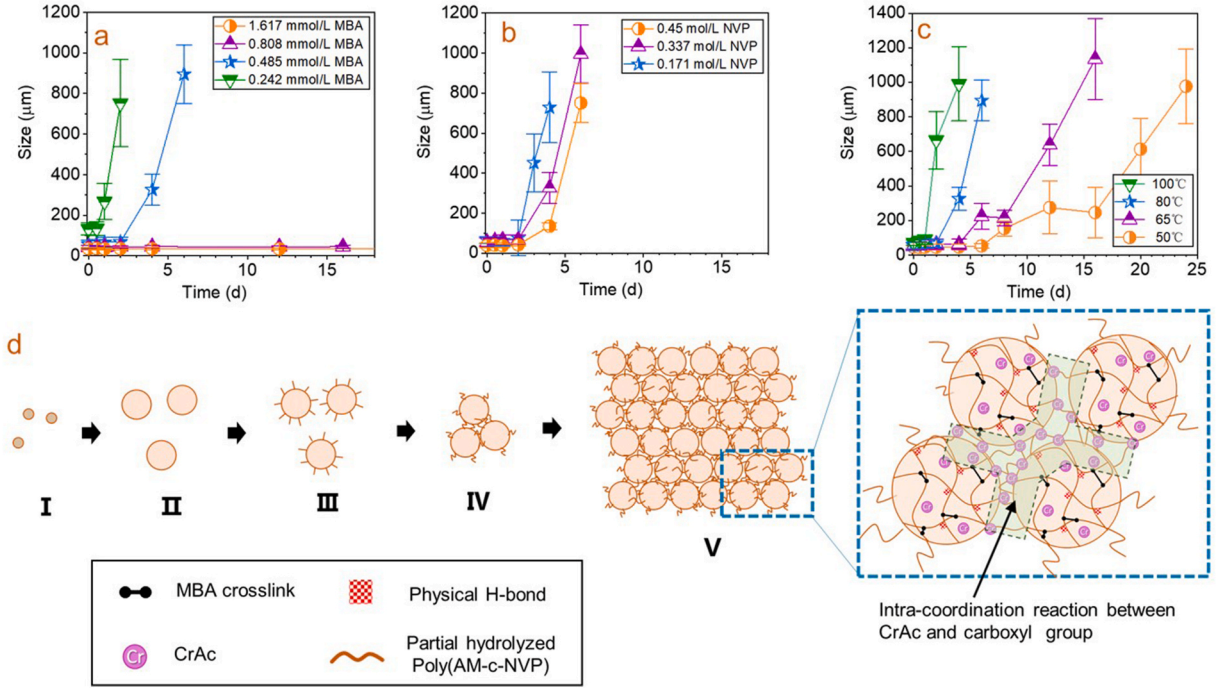

Fig. 5. Size change of the MRPG microsphere dispersion as a function of MBA concentration (a), NVP concentration (b), and temperature (c) and the re-crosslinking stage illustration (d).

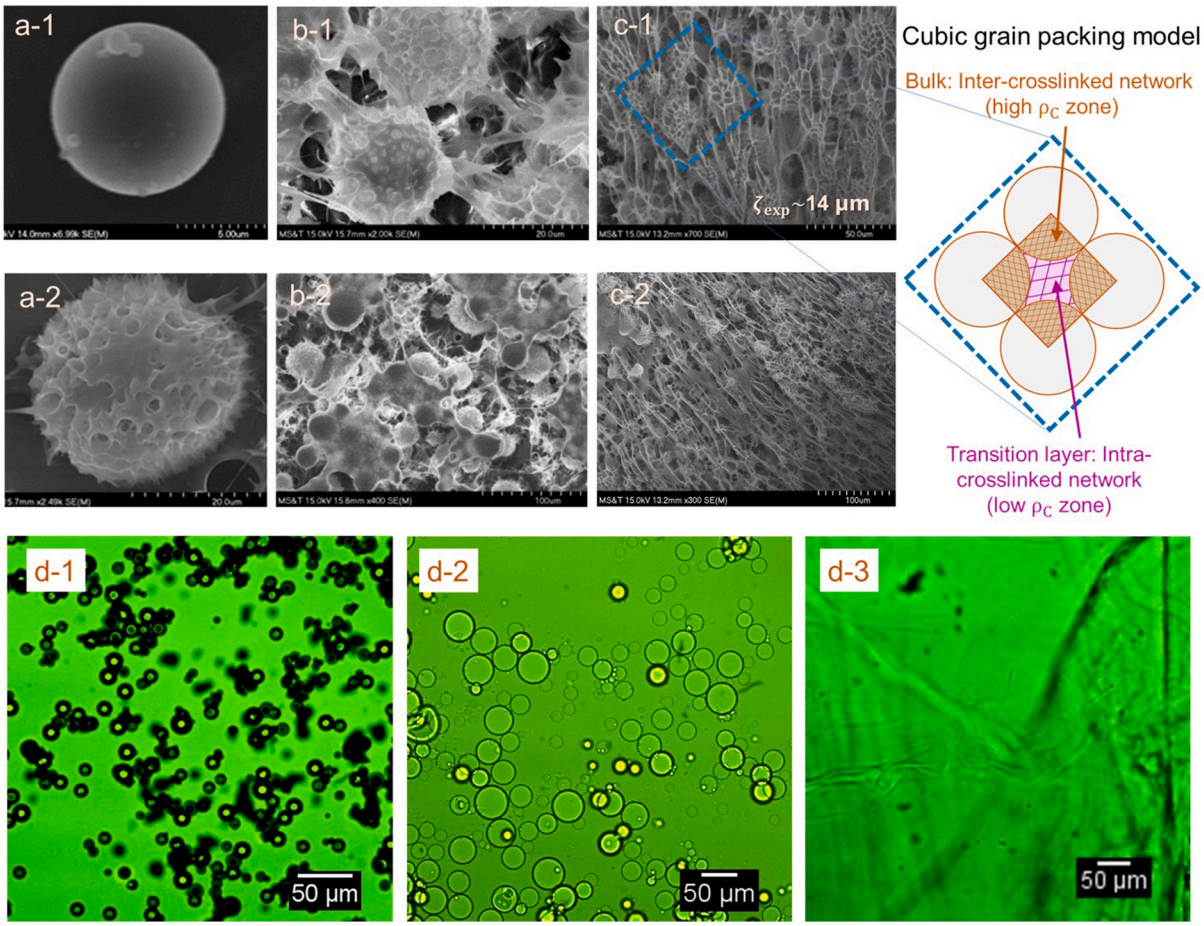

Fig. 6. Morphology of the MRPG microspheres (containing 0.485 mmol/L of MBA and 0.337 mol/L NVP): SEM image of the dry microspheres (a-1), swollen microspheres (a-2), small-scale re-crosslinked microspheres (b-1, b-2), large-scale re-crosslinked microspheres with a cubic grain packing model (c-1, c-2) and CLSM image of microspheres dispersed in acetone (d-1) and 2% NaCl before re-crosslinking (d-2) and in 2% NaCl after re-crosslinking (d-3).

be divided into three stages: from 25 °C to 228 °C, from 228 °C to 335 °C, from 335 °C to 485 °C, and from 485 °C to 690 °C. The proportion of weight loss was small (less than 18% in total) in the first and fourth phases. The evaporation of bound water and the thermal-decomposition of some AM groups on the surface of the poly(AM-c-NVP) polymers caused the weight loss in the first phase (11.87%). More than 62% weight loss occurred in the second and third phases because the amorphous polymers inside the microspheres began to crack and self-decompose as the temperature increased. The AM series inside the microspheres started to degrade first which mainly contributed to the second phase weight loss. NVP series had highly thermal-stability and the decomposition occurred in the third phase. Owing to the introduction of the large lateral pyrrole ring monomer NVP with temperature resistance, the polymer microspheres exhibited effective temperature resistance.

3.5. Migration properties and deformability through membrane pores

An apparatus with a nuclear pore film is most suitable for the study of the migration mechanism. The film had well-proportioned cylindrical pores that can well match the spherical microspheres. The above apparatus was described in detail in a previous article (Pu et al., 2019b). A certain matching relationship existed between the sizes of the microspheres and the film pores, and the threshold pore size could be obtained from the study of the filtration curves. The migration properties of the microspheres with the dry size of 9 μm were investigated. Fig. 4d shows the change in filtration volume as a function of time when the brine-dispersed microsphere system (100 mg/l) aged for 2 h at room temperature (25 °C) was transported through the nuclear pore film with different diameters. After the spurt loss stage that caused 5 ml of the dispersion to pass through the film pores directly, the filtration rates of the microsphere dispersion varied for different films. Given that all the pore sizes of the membranes were smaller than the swollen microsphere (48 μm), this experiment proved the deformability capability of the microsphere. The microspheres passed through the films as the diameters of the film pores decreased from 10 μm to 3 μm. For example, for the 3 μm film, the filtration time was less than 10 min, and approximately 29 ml of the microsphere dispersion transported through the film. The result indicated that the film with pore diameters of 3–10 μm matched the experimental microspheres best. However, when the film pore size was reduced to 1.2 μm, the filtration rate decreased dramatically, and the final filtration time exceeded 35 min given that only 16 ml of the microsphere dispersion passed through the film. Therefore, 3 μm was the minimum pore size for the microsphere to transport and the ratio of microsphere size to pore size was 16:1.

3.6. Re-crosslinking properties of the microspheres

Re-crosslinking properties of the swollen microspheres were evaluated through size measurements in 2% NaCl brine and the re-crosslinking time was obtained when the measured size of the nanocapsule increased for the first time. The MRPG microspheres fabricated with different MBA concentrations of 0.242–1.617 mmol/L were evaluated at 80 °C as shown in Fig. 5a. The result showed that the sizes of the samples with MBA concentration of 0.242 mmol/L and 0.485 mmol/L strongly increased on different days, representing the re-crosslinking

occurred at 0.8 days and 3.5 days respectively. However, the sizes of the samples with 0.808 mmol/L and 1.617 mmol/L MBA didn't change in 16 days, depicting that the microspheres lost capability of re-crosslinking with high MBA concentration. After combing the results with the ρ_C value in Table 2, it was found that the threshold ρ_C to release re-crosslinking of the microsphere was 0.91×10^{15} for the MRPG microsphere.

The effect of NVP concentration on re-crosslinking time was investigated as shown in Fig. 5b. It was noted that the re-crosslinking time for the samples with 0.171, 0.337, and 0.45 mol/L were 2, 2.2, and 3.5 days, respectively, indicating the delaying re-crosslinking property of NVP monomer. The H-bond between large lateral pyrrole rings and amide groups reduced the hydrolysis of the amide group. Therefore, the formation of carboxyl groups was slowed down, resulting in delaying the re-crosslinking of the microspheres. It was noted that the effect of NVP concentration on re-crosslinking time was less important than crosslinker MBA.

The swollen microspheres were aged at different temperature (50 °C, 65 °C, 80 °C, and 100 °C), as shown in Fig. 5c, to obtain the size changes which reflected the effect of temperature on re-crosslinking time. It was found that temperature strongly influenced the re-crosslinking time. As a result, the re-crosslinking time gradually decreased from 16.5 days to 1 day as the temperature was increased from 50 °C to 100 °C. Interestingly, a unique plateau was found for the sample at 65 °C and 50 °C, indicating a midterm stage was existed when the re-crosslinking reaction was slowed down at low temperature.

The different re-crosslinking stages of the microspheres were depicted as shown in Fig. 5d. The morphologies of the microspheres at different stages were observed using SEM and CLSM as demonstrated in Fig. 6. The microspheres remained monodispersed at the dry phase (stage I) as shown in Fig. 6a-1a-1 and Fig. 6d–1. In brine solution, the microspheres absorbed water and transformed into large spheres with a three-dimensional network morphology (stage II). The swollen microspheres presented a regular porous structure (Fig. 6a–2) and maintained a stable swelling ratio in brine (Fig. 6d–2). As the increased absorption of water, amide groups started to hydrolyze to form carboxyl group, resulting in decreasing the inner H-bond number of the microsphere. Therefore, the microsphere might become softer and the surface polymer started to be waivable (stage III). Subsequently, CrAc, on the surface polymer, could form intra-coordinated physical bond with other microspheres (Fig. 5d green area) to form an intra-complex structure and made the microspheres to aggregate with each other (stage IV). The microspheres transformed into sea urchin-like structures with outstretched polymer chains that induced re-crosslinking on a small scale at first and caused the microspheres to approach each other as illustrated in Fig. 6b–1 and 6b-2. At the final stage (stage V), a large bulk gel with a large-scale unique binary network pattern formed among the microspheres. Fig. 6c–1, 6c-2, and 6d-3 illustrate the formation of a bulk gel. The binary network pattern demonstrated two different interlaced crosslinks as shown in Fig. 6c–1 right part: The high ρ_C zones of the crosslinks were contributed by the body of the original microspheres with covalent MBA crosslinks and CrAc inter-coordination bonds, called bulk part; The low ρ_C zones ($\zeta_{exp} \sim 14$ μm) of the bare CrAc intra-coordination bonds, called transition layer.

Our previous research on microspheres showed that the swollen nanoparticles and microspheres presented good deformability that enabled the tight packing of the microspheres (Pu et al., 2019b). Therefore, a grain packing model was constructed to understand the two-level network structure and related parameters further (Fig. 6c–1 right part). The cubic area was selected, and the ratio of two different network volumes was obtained through volume calculation. For example, for a cubic packing model, the proportions of the intercrosslinked network and the intracrosslinked network were 52.4% and 47.6%, respectively. The intercrosslinked network formed through MBA covalent bonding and chromium acetate complexation exhibited high crosslinking density ($\rho_{C,1}$). By contrast, the other network showed low crosslinking density ($\rho_{C,2}$) (Wang et al., 2018c). The network parameters of both network structures were calculated by using Equations (3)–(8), and the results are shown in Table 3. ζ_{exp} ~14 μm was used to calculate $\phi_{p,m,2}$ through the dichotomy method. $\rho_{C,1}$ was found to be about 90 times of $\rho_{C,2}$. This result showed that the intensity of MBA crosslinking was considerably stronger than that of chromium acetate complexation. For the isodiametric microspheres, six standard packing types were studied, and the final average molecular weight between crosslinks ($\overline{M_{total}}$) and crosslinking density (ρ_{total}) were calculated as shown in Table 4. The study on irregular MRPG microspheres in consideration of deformability and degradation is ongoing and will be reported in the future.

Table 3
Network parameters of two network zones of re-crosslinked MRPG microspheres ($\chi = 0.5042$).

Intercrosslinked network zone		Intracrosslinked network zone	
$\mathbf{m_{w,1}}$ **(V/V)**	83.1	$m_{w,2}$ (V/V)	151.7
$\boldsymbol{\zeta_{exp,1}}$ **(nm)**	1443.5	$\zeta_{exp,2}$ (nm)	14000
SR	79.9	SR	145.1
$\boldsymbol{\phi_{p,m,1}}$ **(×10^{-2})**	1.3	$\phi_{p,m,2}$ (× 10^{-2})	0.7
$\overline{\mathbf{M_1}}$ **(×10^{7})**	6.31	$\overline{M_2}$ (× 10^{7})	57.0
$\boldsymbol{\rho_{C,1}}$ **(×10^{15})**	0.91	$\rho_{C,2}$ (× 10^{15})	0.1

4. Conclusion

In summary, the novel dual chemical and physical crosslinked microsphere (MRPG) was fabricated via radical suspension copolymerization of AM and NVP monomers in presence of MBA and subsequent introduction of CrAc. Together with the strong crosslinking through a chemical covalent bond of MBA, H-bond triggered between pyrrole ring and amide group formed the weak crosslinking which was anticipated to prohibit the hydrolysis of the amide group. The H-bond delayed the formation of CrAc coordination bond by delaying the formation of carboxyl groups, resulting in achieving the re-crosslinking of the microspheres (controlled from 0.8 days to 16.5 days). As a result, the delayed formation of intra-coordination bonds was expected to endow the microspheres with re-crosslinking ability, upon swelling and deformability. As a result, the microspheres exhibit the tunable initial size (8–165 μm) and swelling ratio (30–630 μm) with variable concentration of MBA, NVP, and fabrication stirring rate, with controllable network parameters. The SR was controlled up to 93.5. With the existence of pyrrole ring and H-bond, the microspheres showed high temperature resistance (less than 12% weight loss at 200 °C), with high migration ability which can transport through 1/16 size of microsphere itself. The long re-crosslinking time and other comprehensive properties broaden the use of the MRPG microspheres.

Credit author statment

Jingyang Pu: Conceptualization, Writing – original draft, Formal analysis, Funding acquisition. **Baojun Bai**: Conceptualization, Writing – review & editing. **Jiaming Geng**: Supervision, Validation. **Na Zhang**: Data curation, Funding acquisition, Supervision. **Thomas Schuman**: Validation.

Declaration of competing interest

The authors declare that they have no known competing financial interests or personal relationships that could have appeared to influence the work reported in this paper.

Table 4
Total network parameters of MRPG microspheres.

Standard Packing type	Vertical view	3-D view	A1 (%)	A2 (%)	$\overline{M_{total}}$ ($\times 10^7$)	ρ_{total} ($\times 10^{15}$)
Cubic			52.4	47.6	30.4	0.1
Hexagonal	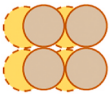	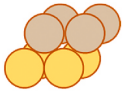	60.5	39.5	26.3	0.1
Rhombohedral	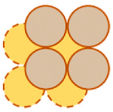	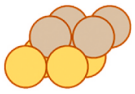	74.0	26.0	19.5	0.1
Orthorhombic		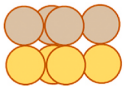	60.5	39.5	26.3	0.1
Tetragonal		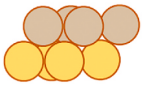	69.8	30.2	21.6	0.1
Triclinic		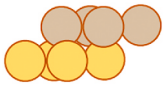	74.0	26.0	19.5	0.1

Data availability

No data was used for the research described in the article.

Acknowledgements

Funding for this study was provided by ConocoPhillips and Occidental Petroleum. This paper reflects the views of the authors and does not necessarily reflect the views of the other companies. The authors would also like to thank all the lab personnels who contributed to work efforts discussed in this paper.

The paper was written after the first author joined China University of Petroleum (Beijing). The project was supported by the National Natural Science Foundation of China (grant number 52104057 and 52204041) and Natural Science Foundation of Shandong Province (grant number ZR2021QE106 and ZR2021QF076) when writing this paper.

References

Bai, B., Zhou, J., Yin, M., 2015. A comprehensive review of polyacrylamide polymer gels for conformance control. Petrol. Explor. Dev. 42 (4), 525–532.
Çaykara, T., Turan, E., 2006. Effect of the amount and type of the crosslinker on the swelling behavior of temperature-sensitive poly(N-tert-butylacrylamide-co-acrylamide) hydrogels. Colloid Polym. Sci. 284 (9), 1038–1048.
Flory, P.J., Rehner, J., 1943. Statistical mechanics of cross-linked polymer networks I. Rubberlike elasticity. J. Chem. Phys. 11 (11), 512–520.
Gales, J., Young, T., Willhite, G., Green, D., 1994. Equilibrium swelling and syneresis properties of Xanthan gum-Cr (III) gels. SPE Adv. Technol. 2 (2), 190–198.
Gao, Y., Peng, X., Wu, Q., Yang, D., Wang, W., Peng, Q., Wang, T., Wang, J., Liu, J., Zhang, H., Zeng, H., 2022. Hydrogen-bonding-driven multifunctional polymer hydrogel networks based on tannic acid. ACS Applied Polymer Materials 4 (3), 1836–1845.
Guo, Z., Gu, H., He, Y., Zhang, Y., Xu, W., Zhang, J., Liu, Y., Xiong, L., Chen, A., Feng, Y., 2020. Dual dynamic bonds enable biocompatible and tough hydrogels with fast self-recoverable, self-healable and injectable properties. Chem. Eng. J. 388, 124282.
Hu, C., Long, L., Cao, J., Zhang, S., Wang, Y., 2021. Dual-crosslinked mussel-inspired smart hydrogels with enhanced antibacterial and angiogenic properties for chronic infected diabetic wound treatment via pH-responsive quick cargo release. Chem. Eng. J. 411, 128564.
Li, B., Han, Y., Zhang, Y., Cao, X., Luo, Z., 2020. Dual physically crosslinked nanocomposite hydrogels reinforced by poly(N-vinylpyrrolidone) grafted cellulose nanocrystal with high strength, toughness, and rapid self-recovery. Cellulose 27 (17), 9913–9925.
Lin, M., Zhao, Q., Dang, S., Wang, Y., Wang, Y., Wang, X., 2015. Preparation and properties of terpolymeric microspheres for deep profile control in oilfields. Mater. Res. Innovat. 19 (5), 574–579. S5-S S5-.
Lv, C., Liao, X., Zou, F., Tang, W., Xing, S., Li, G., 2022. Generating porous polymer microspheres with cellular surface via a gas-diffusion confined scCO2 foaming technology to endow the super-hydrophobic coating with hierarchical roughness. Chem. Eng. J., 136192
Mandal, B., Ray, S.K., 2013. Synthesis of interpenetrating network hydrogel from poly (acrylic acid-co-hydroxyethyl methacrylate) and sodium alginate: modeling and kinetics study for removal of synthetic dyes from water. Carbohydr. Polym. 98 (1), 257–269.
Mandal, B., Ray, S.K., Bhattacharyya, R., 2012. Synthesis of full and semi Interpenetrating hydrogel from polyvinyl alcohol and poly (acrylic acid-co-hydroxyethylmethacrylate) copolymer: study of swelling behavior, network parameters, and dye uptake properties. J. Appl. Polym. Sci. 124 (3), 2250–2268.
Pu, J., Geng, J., Bai, B., 2018. Effect of the chromium ion diffusion in polyacrylamide/chromium acetate gelation system with surrounding water on gelation behavior. J. Petrol. Sci. Eng. 171, 1067–1076.
Pu, J., Bai, B., Alhuraishawy, A., Schuman, T., Chen, Y., Sun, X., 2019a. A recrosslinkable preformed particle gel for conformance control in heterogeneous reservoirs containing linear-Flow Features. SPE J. 24 (4), 1714–1725.
Pu, J., Geng, J., Han, P., Bai, B., 2019b. Preparation and salt-insensitive behavior study of swellable, Cr 3+ -embedded microgels for water management %J. J. Mol. Liquids 273.
Pu, J., Geng, J., Han, P., Bai, B., 2019c. Preparation and salt-insensitive behavior study of swellable, Cr3+-embedded microgels for water management. J. Mol. Liq. 273, 551–558.
Pu, J., Bai, B., Schuman, T.P., 2021a. Systematic evaluation of a novel self-healing poly (acrylamide-co-vinyl acetate)/alginate polymer gel for Fluid Flow control in high temperature and high salinity reservoirs. Polymers 13 (21).
Pu, J., Gu, X., Luo, M., Bai, Y., 2021b. Polyelectrolyte complex induced Stimuli-responsive Self-association and reinforcement of interpenetrated Poly(acrylamide-co-vinyl acetate)/alginate particles for fossil energy recovery. J. Mol. Liq. 343, 117596.
Rebers, L., Reichsöllner, R., Regett, S., Tovar, G.E.M., Borchers, K., Baudis, S., Southan, A., 2021. Differentiation of physical and chemical cross-linking in gelatin methacryloyl hydrogels. Sci. Rep. 11 (1), 3256.
Samanta, H.S., Ray, S.K., 2014. Synthesis, characterization, swelling and drug release behavior of semi-interpenetrating network hydrogels of sodium alginate and polyacrylamide. Carbohydr. Polym. 99, 666–678.
Song, D., Jia, Y., Yu, L., Chen, H., Wang, T., Lin, G., 2008. Further enhanced oil recovery by using polymer minispheres at Gudao oil field after polymer flood. Oilfield Chem. 2, 18.
Sudha, M., Rajarajan, M., 2013. Deactivation of Photocatalytically Active ZnO Nanoparticle by Surface Capping with Poly Vinyl Pyrrolidone, vol. 3, pp. 45–53.
Varel, F.T., Dai, C., Shaikh, A., Li, J., Sun, N., Yang, N., Zhao, G., 2021. Chromatography and oil displacement mechanism of a dispersed particle gel strengthened Alkali/Surfactant/Polymer combination flooding system for enhanced oil recovery. Colloids Surf. A Physicochem. Eng. Asp. 610, 125642.

Wan, T., Huang, R., Zhao, Q., Xiong, L., Luo, L., Tan, X., Cai, G., 2013. Synthesis and swelling properties of corn stalk-composite superabsorbent. J. Appl. Polym. Sci. 130 (1), 698–703.
Wang, L., Long, Y., Ding, H., Geng, J., Bai, B., 2017. Mechanically robust re-crosslinkable polymeric hydrogels for water management of void space conduits containing reservoirs. Chem. Eng. J. 317, 952–960.
Wang, Z., Lin, M., Gu, M., Dong, Z., Zhang, J., Yang, Z., 2018a. Zr-Induced high temperature resistance of polymer microsphere based on double crosslinked structure. RSC Adv. 8 (35), 19765–19775.
Wang, X.-H., Song, F., Qian, D., He, Y.-D., Nie, W.-C., Wang, X.-L., Wang, Y.-Z., 2018b. Strong and tough fully physically crosslinked double network hydrogels with tunable mechanics and high self-healing performance. Chem. Eng. J. 349, 588–594.
Wang, L., Long, Y., Bai, B., 2018c. Low temperature applicable polyelectrolyte gelator to covalently bridged partially hydrolyzed poly(acrylamide) in situ gel for fossil energy recovery. Chem. Eng. J. 334, 2558–2567.
Wang, H., Lin, M., Dong, Z., Xu, C., Xue, R., Yang, Z., 2020a. Study on the association behavior of synthesized hydrophobically associating polymer microspheres. Colloids Surf. A Physicochem. Eng. Asp. 598, 124829.
Wang, H., Lin, M., Zhao, Q., Xu, C., Dong, Z., Yang, Z., Zhang, J., 2020b. Fabrication, formation mechanism, and thermal degradation process of AM/AMPS/NVP terpolymeric microspheres with different microstructures. Colloids Surf. A Physicochem. Eng. Asp. 589, 124401.
Wang, Z.-Y., Lin, M.-Q., Li, H.-K., Dong, Z.-X., Zhang, J., Yang, Z.-H., 2021a. Plugging property and displacement characters of a novel high-temperature resistant polymer nanoparticle. Petrol. Sci. 19 (1), 387–396.
Wang, Z., Lin, M., Dong, Z., Zhang, J., Yang, Z., 2021b. Synthesis and radiation grafting modification of hydroxyl controlled AM/HEMA polymer microspheres. J. Dispersion Sci. Technol. 42 (7), 1031–1041.
Wang, R., Bi, S., Guo, Z., Feng, G., 2022. Molecular insight into replacement dynamics of CO2 enhanced oil recovery in nanopores. Chem. Eng. J. 440, 135796.
Xu, J., Cheng, J., Wang, Y., Yang, W., Park, J.-Y., Kim, H., Xu, L., 2021. Strengthening CO2 dissolution with zeolitic imidazolate framework-8 nanoparticles to improve microalgal growth in a horizontal tubular photobioreactor. Chem. Eng. J. 405, 126062.
Yao, C., Lei, G., Hou, J., Xu, X., Wang, D., Steenhuis, T.S., 2015. Enhanced oil recovery using micron-size polyacrylamide elastic microspheres: underlying mechanisms and displacement experiments. Ind. Eng. Chem. Res. 54 (43), 10925–10934.
Zhang, H., Yang, H., Sarsenbekuly, B., Zhang, M., Jiang, H., Kang, W., Aidarova, S., 2020. The advances of organic chromium based polymer gels and their application in improved oil recovery. Adv. Colloid Interface Sci. 282, 102214.
Zhao, Y., Bai, B., 2022a. Selective penetration behavior of microgels in superpermeable channels and reservoir matrices. J. Petrol. Sci. Eng. 210, 109897.
Zhao, Y., Bai, B., 2022b. Experimental study of transport behavior of swellable microgel particles in superpermeable channels for conformance control. SPE J. 27 (1), 790–805.
Zhao, Y., Leng, J., Lin, B., Wei, M., Bai, B., 2021a. Experimental study of microgel conformance-control treatment for a polymer-flooding reservoir containing superpermeable channels. SPE J. 26 (4), 2305–2317.
Zhao, Y., Wei, M., Leng, J., Bai, B., 2021b. Propagation of swellable microgels through superpermeable channels: impact of particle–pore matching size relationship. Energy Fuels 35 (22), 18533–18542.
Zhu, D., Hou, J., Chen, Y., Zhao, S., Bai, B., 2018. In situ surface decorated polymer microsphere technology for enhanced oil recovery in high-temperature Petroleum reservoirs. Energy Fuels 32 (3), 3312–3321.